Journal of Alloys and Compounds 514 (2012) 54–59

Contents lists available at SciVerse ScienceDirect

Journal of Alloys and Compounds

journal homepage: www.elsevier.com/locate/jallcom

Combination of mechanochemical activation and self-propagating behavior for the synthesis of nanocomposite Al_2O_3/B_4C powder

Reza Ebrahimi-Kahrizsangi*, Omid Torabi

Advanced Materials Research Center, Materials Engineering Department, Najafabad Branch, Islamic Azad University, Isfahan, Iran

ARTICLE INFO

Article history:
Received 1 August 2011
Received in revised form 21 October 2011
Accepted 21 October 2011
Available online 7 November 2011

Keywords:
Composite materials
Powder metallurgy
Mechanochemical processing
X-ray diffraction
Thermal analysis

ABSTRACT

In this research, Al_2O_3/B_4C nanocomposite was successfully synthesized by combining of mechanically induced self-propagating reaction of aluminum, graphite and boric acid powders mixture. For this purpose the starting materials were activated in a planetary ball mill under Argon atmosphere. The structural evaluation of powder particles was investigated by X-ray diffraction, FTIR spectrometer and scanning electron microscopy (SEM). The effect of activation time on the combustion temperature and the reaction products was discussed based on STA experiments. The results indicated that the reaction between Al and B_2O_3 (aluminothermic reaction) is highly exothermic and should be in combustion mode. According to XRD analyses, the Al_2O_3/B_4C nanocomposite was fabricated after 4 h of high energy ball milling. Simultaneous thermogravimetric analyzer (STA) results showed that increasing the activation time to 3 h can decrease the temperature of combustion reaction to590 °C. SEM observations confirmed that the range of particle size was within 100 nm.

1. Introduction

Due to excellent properties such as high hardness and wear resistance, good thermal conductivity and high temperature stability, Alumina (Al_2O_3) is the most cost effective and widely used material in the family of engineering ceramics [1,2]. However, low fracture toughness and poor thermal shock resistance limited the use of single phase alumina. These disadvantages were improved by incorporating a second phase as reinforcement such as SiC, ZrO_2, TiB_2 and others into the base material to form alumina-matrix composites [2–4]. In addition, the promising increase in strength and thermal shock resistance is the greatest benefit of ceramic nanocomposites. Grain refinement, flaw reduction, subgrain formation and residual stress are some factors depending on the composition and microstructure to improve mechanical and thermal properties [5]. As a result, another mechanism to overcome these disadvantages is to fabricate alumina matrix nanocomposite.

Traditionally, in the ex situ particulate-reinforced, the reinforcement is prepared separately and then mixed with the matrix by different methods such as powder metallurgy, casting route, spray deposition and others [6]. Non-wetting of reinforcement with the matrix, contaminated matrix–reinforcement interfaces and scale of the reinforcing phase are some limitations to the use of these methods. In recent years, efficient techniques involving the in situ generation of the reinforcing phase have been developed to fabricate metal or ceramic base nanocomposites. In situ methods are founded on chemical reactions between elements or between element and compound during the composite fabrication [7]. Due to good thermodynamic stability, strong interfacial bonding, finer size and appropriate distribution which give better mechanical features, in situ process attracts much attention [6,7]. Mechanochemical activation is a solid state powder processing method which involves inducing chemical reactions in a mixture of reaction powders at room temperature or at least much lower temperatures. An increase in the kinetic of reaction during high energy milling can be a result of microstructural refinement, repeated cold deformation and fracture of particles. In recent years, the mechanochemical technique has been widely used to fabricate interpenetrating phase composites with nanosized microstructures [4,8].

Boron carbide (B_4C) is a suitable choice as the second phase because of high melting point, excellent hardness, low specific density (2.52 g/cm^3), high elastic modulus and high chemical stability [9]. Previous studies have showed that the addition of 10–20 vol% B_4C whiskers to alumina matrix increased fracture toughness up to 6.2 MPa. [10]. Also, Jung et al. proved that the addition of B_4C particles to monolithic Al_2O_3 increased the micro-hardness and decreased the grain size of the composites, therefore, improving its cutting performance, compared to the inserts prepared from monolithic pressureless sintered Al_2O_3 [11]. Yi et al. investigated the fabrication of highly porous boron carbide–aluminum oxide ceramic composites by combustion synthesis process [12]. Yonghe et al. studied thermodynamics of Al_2O_3/B_4C composite synthesized via SHS technique starting with Al, B_2O_3 and C [13]. They

* Corresponding author. Tel.: +98 331 229 1008; fax: +98 331 229 1008.
E-mail address: rezaebrahimi@iaun.ac.ir (R. Ebrahimi-Kahrizsangi).

0925-8388/$ – see front matter © 2011 Elsevier B.V. All rights reserved.
doi:10.1016/j.jallcom.2011.10.075

reported that the adiabatic temperature for thermite SHS system $4Al + B_2O_3 + C$ by "CALPHAD" method is significantly lower than that obtained by conventional method [13]. In addition, the aluminum borate in the form of $9Al_2O_3 \cdot 2B_2O_3$ is detected as a major by-product in this method [14]. Therefore, due to above disadvantages and some problems in SHS process such as grain growth, non-uniform phase and others, it is necessary to find an effective technique that could overcome disadvantages to fabricate the applicable nanocomposite material of Al_2O_3/B_4C with high purity.

In this work, synthesis of ceramic matrix nanocomposite powder Al_2O_3/B_4C was carried out via mechanochemical method by using $Al–H_3BO_3–C$ as precursor materials at room temperature. Also, the effect of high energy milling time on reaction temperature, the structural evolution and formation mechanism of Al_2O_3/B_4C nanocomposite were investigated in detail.

2. Experimental work

The precursor materials were aluminum (Merck, 99.7% purity, particles size 40 ± 5 μm), boric acid (Merck, 99.95% purity, mean particles size 30 ± 5 μm) and graphite (Merck, 99.5% purity, mean particles size 50 μm). For the fabrication of the nanocomposite, a distinct amount of aluminum was mixed with boric acid (H_3BO_3) and carbon according to the following reactions:

$$2H_3BO_3 = B_2O_3 + H_2O \quad (1)$$

$$4Al + 2B_2O_3 + C = 2Al_2O_3 + B_4C \quad (2)$$

The precursor materials were milled in a planetary ball mill for 2, 3, 4 and 10 h at room temperature. Details of ball mill machine and milling conditions are given in Table 1. To prevent the oxidation process, the vial of milling was filled by high purity argon gas before ball milling.

XRD analysis was carried out using Cu-K_α radiation to identify different phases of the starting powders and mechanically alloyed powders. The diffractometer (Philips X-ray diffractometer) was operated at 40 kV and 30 mA. Scans were performed between $10^\circ < 2\theta < 90^\circ$. "PANalytical X'Pert HighScore" software was also used for the analysis of different peaks. The diffraction patterns of products were compared to proposed standards by the Joint Committee on Powder Diffraction and Standards (JCPDS). Fourier transform infrared (FTIR) spectra of the samples were performed using FT-IR-6300/JASCO. A scan range in the wave number of 4000–400 cm^{-1} with a resolution of 2 cm^{-1} has been found to be adequate. The reaction process and features were also investigated by thermal analyses (TG–DTA; model BÄHR 503). A small amount of the reactants weighing about 50 ± 5 mg were held in an alumina crucible and heated under argon flow (flow rate: 50 ml/min) at a heating rate of 10 °C/min up to 1100 °C. The morphology and the agglomerate size distribution of the milled powders were studied by field emission scanning electron microscopy (FE-SEM, Hitachi 4160, 15 kV).

Table 1
Details of ball mill machine and milling conditions.

Rotation speed of vial (rpm)	500
Diameter of vial (mm)	100
Vial material	Hardened chromium steel
Ball material	Hardened carbon steel
Diameter of balls (mm)	20
Number of balls	5
Balls to powder weight ratio	20:1
Total powder mass (g)	7

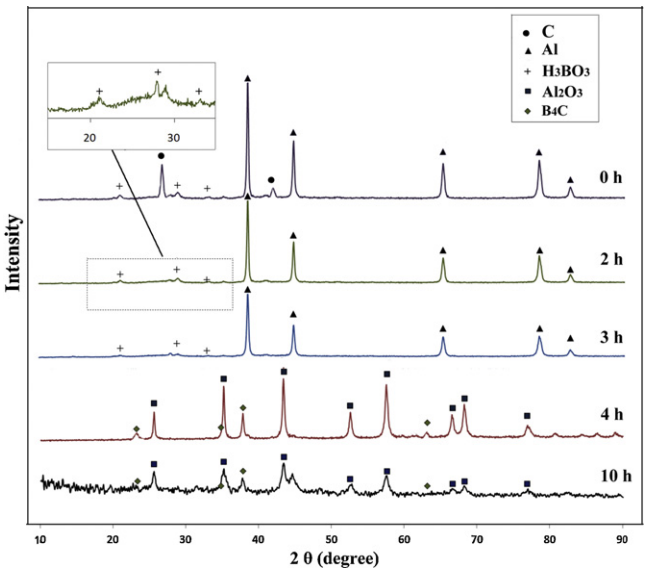

Fig. 1. XRD patterns of samples milled for 0 (as a reference), 2, 3, 4 and 10 h.

3. Result and discussion

3.1. Phase detection (XRD and FTIR analysis)

Fig. 1 shows the XRD patterns of $Al–H_3BO_3–C$ powder mixture, mechanically alloyed for 0 (as a reference), 2, 3, 4 and 10 h. In the XRD pattern of starting powder mixture, all the sharp peaks correspond to Al, and those corresponding to H_3BO_3 and C have low intensity. Lack of graphite peaks in the sample milled for 2 h can be related to transformation of crystal state of graphite into amorphous state as reported in some investigations [15]. No tangible changes were observed in XRD pattern of sample milled for 3 h thus, indicating that no new phases were formed during milling process. In the XRD pattern obtained after 4 h milling process, the peaks of precursor materials disappeared completely. Meanwhile, new sharp peaks appear to emerge, corresponding to the formation of Al_2O_3 (JCPDS: 01-075-1865). In addition, three peaks at $2\theta = 23.329^\circ$, $2\theta = 37.768^\circ$ and $2\theta = 63.061^\circ$ corresponding to the formation of B_4C (JCPDS: 00-001-1163) that cannot be detected easily due to intense Al_2O_3 peaks can be observed. Further milling process up to 10 h had no special effect except broadening of Bragg peaks which is ascribed by decreasing in crystallite size as well as lattice strain induced in the powder particles [16]. It is reported that the formation of by-products such as AlB_{10}, AlB_{12}, $9Al_2O_3 \cdot 2B_2O_3$ and others is the main problem in the synthesis of Al_2O_3/B_4C composite via combustion methods [13,14]. It should be mentioned that in Fig. 1 no traces of undesirable phases were observed in XRD patterns during milling.

In order to confirm the results of X-ray pattern, two samples milled for 3 and 4 h were analyzed with FTIR spectrometer. Fig 2(a) indicates several absorption peaks which are assigned to the spectrum of boric acid. Absorption peaks at around 1198 and 1450 cm^{-1} refer to B–OH and B–O stretching vibration, respectively [17,18]. Therefore, no product phases could be detected in the sample milled for 3 h. As can be seen in Fig. 2(b), the sample milled for 4 h shows two peaks at around 1100 and 1270 cm^{-1} which are the characterizing absorption peaks of B–C bond and boron carbide [19,20]. The broad features in the range of 450–1000 cm^{-1} represented the characteristic of aluminum oxide [21,22]. In addition, broad absorption band in the range of 588–830 cm^{-1} was due to Al–O stretching vibrations. FTIR results suggested that Al_2O_3/B_4C composite

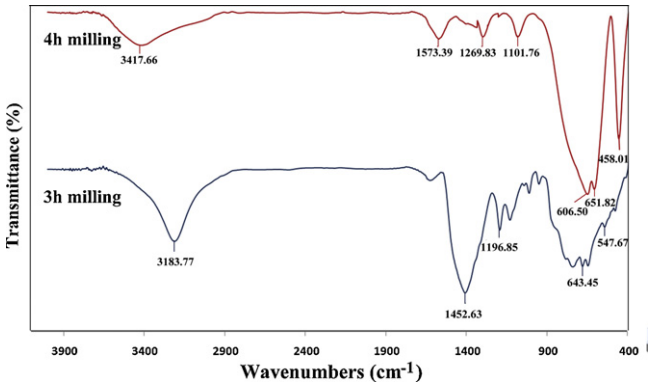

Fig. 2. FTIR spectra of samples milled for 3 and 4 h.

powder was formed after 4 h milling process as estimated in the X-ray pattern.

3.2. Thermodynamic consideration

Although the interpretation on thermodynamic behavior of in situ solid state reactions such as mechanical activation is not completely studied, using some usual thermodynamic relations could help to know the basic information about reactions and to estimate their behavior during the process. Al_2O_3/B_4C nanocomposite may be synthesized via two stages: in the first stage, reduction of B_2O_3 by Al and/or C to produce elemental boron as presented in reactions (3) and/or (4).

$$2Al + B_2O_3 = 2[B] + Al_2O_3 \quad (3)$$

$$\Delta H^0_{298} = -420.5 \ \text{KJ/mole} \quad \Delta G^0_{298} = -404.70 \ \text{KJ/mole}$$

$$B_2O_3 + 3C = 2[B] + 3CO \quad (4)$$

$$\Delta H^0_{298} = +748.52 \ \text{KJ/mole} \quad \Delta G^0_{298} = +725.8 \ \text{KJ/mole}$$

In the second stage, the elemental boron [B] reacts with remaining C to form B_4C according to reactions (5).

$$4[B] + C = B_4C \quad (5)$$

$$\Delta H^0_{298} = -62.05 \ \text{KJ/mole} \quad \Delta G^0_{298} = -61.31 \ \text{KJ/mole}$$

In spite of reaction (4), during ball milling at room temperature, reactions (3) and (5) can thermodynamically be possible to occur due to the negative standard Gibbs free energy of reactions. Negative standard enthalpy of formation at 298 K of these two reactions indicates that these reactions are exothermic, but carbothermic reaction (4) is sensitively endothermic. However, the occurrence of these reactions at room temperature is limited by kinetic conditions. In this regard, mechanical activation process can enhance the kinetics of the reduction reactions. This can be related to the following reasons: (i) new surfaces were created by reduction in the average particle size during repeated welding and fracturing of powder particles (ii) decrease in the diffusion distances by accumulation of defects (point defects specially vacancy, dislocations and grain boundaries), high strain, creation of fresh surface and distribution of particles during the ball milling process (iii) local temperature increasing [8,16].

Depending on the milling conditions and enthalpy of reaction, mechanochemical reactions fall into two categories: progressive reaction and mechanically induced self-sustaining reaction (MSR). In the first type, the synthesis of final products extends to a very small volume slowly during each collision between the milled material and the grinding medium that contributes to the comminution, mixing, and defect formation [6,8]. In the second type, a self-propagating combustion reaction is initiated after a definite amount of milling. During the milling process, intimate contact between the reactant phases is an essential requirement for the self-propagating synthesis. Therefore, occurrence of the combustion reaction causes a rapid rise in temperature at the wall of the mill vial, and provides the conditions for quick transformation [6,8].

This type of reaction mechanism can be predicted by calculating the adiabatic temperature (T_{ad}) or by describing this property ($-\Delta H_{298}/\sum C_p$). For self-sustaining mode reaction to take place it is necessary that these quantities be at least $T_{ad} > 1800$ K and $-\Delta H_{298}/\sum C_p > 2000$ K [23].The value of T_{ad} would be calculated using the equation below:

$$\Delta Q = -\Delta H^0_{298} + \int_{298}^{Tm} \sum C_p(\text{Solid}) \cdot dT + \Delta H_m + \int_{Tm}^{Tad} \sum C_p(\text{Liquied}) \cdot dT = 0 \quad (6)$$

where C_p, and ΔH^0_{298} and ΔQ are specific heat capacity, standard enthalpy changes of formation at 298 K and heat of reaction, respectively.Table 3 shows the T_{ad} and $(\Delta H/C_p)$ for reaction (2), (3) and (5) that were calculated by using thermodynamics data given in Table 2 [24]. The calculated T_{ad} of reactions (2) and (3) are much higher than the critical value of 1800 K. As a result, the initiation of MSR is estimated during ball milling of stoichiometric mixture of Al–B_2O_3–C.

3.3. TG–DTA analysis

DTA and TG techniques were utilized to investigate the reaction mechanism and to study the effect of the activation time on thermite reactions behavior and initial reaction temperature. For this purpose, the Al, H_3BO_3 and C powder mixtures were milled for 0 (unmilling), 1, 2 and 3 h and then subjected to DTA–TG analysis at a heating rate of 10 deg. min^{-1} (Fig. 3). The endothermic peak at ~190 °C in the DTA curve of all samples is related to disintegration

Table 2
Thermodynamics data for B_4C, Al_2O_3, Al, B_2O_3 and C [23].

Phase	Temp. range (K)	ΔH^0_{298} (kJ/mol)	ΔH^0_m (kJ/mol)	C_p (J/mol K)
B_4C	298–1373	−71.56	–	$96.21 + (22.6 \times 10^{-3}T) - (44.86 \times 10^5 T^{-2})$
	1373–3036			131.23
Al_2O_3	298–1800	−1677.77	25.7	$106.6 + (17.78 \times 10^{-3}T) - (28.54 \times 10^5 T^{-2})$
	1800–2327			$127.80 + (5.27 \times 10^{-3}T) - (80.14 \times 10^5 T^{-2})$
	2327–3000			192.46
Al	–	0	–	–
B_2O_3	–	−1272.24	–	–
C	–	0	–	–

Table 3
Value of (T_{ad}) and ($-\Delta H_{298}/\sum C_p$) for reactions (2), (3) and (5).

Reaction	T_{ad} (K)	$-\Delta H_{298}/\sum C_p$ (K)
$4Al + 2B_2O_3 + C = 2Al_2O_3 + B_4C$	~3568	~6600
$2Al + B_2O_3 = 2[B] + Al_2O_3$	~2239	~5272
$4[B] + C = B_4C$	~1423	~1152

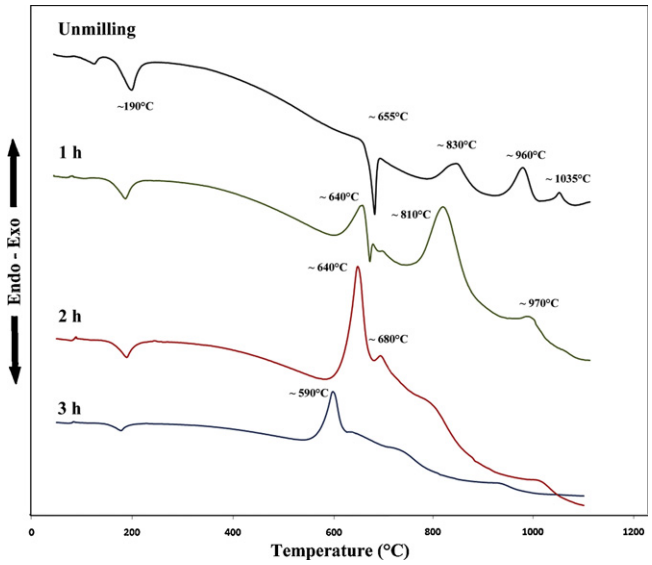

Fig. 3. DTA curves for the $Al + H_3BO_3 + C$ mixtures milled for different times (heating rate 10 deg. min^{-1}).

of boric acid into boron oxide and water vapor according to the following reaction:

$$H_3BO_3 \rightarrow 2HBO_2 + 2H_2O \rightarrow B_2O_3 + H_2O \quad (7)$$

DTA curve of unmilling samples exhibited another endothermic peak at about 655 °C related to melting of metal Al powder. This curve also shows three exothermic peaks, around 830, 960 and 1035 °C. In order to make clear the reactions which occurred within exothermic peaks, after DTA analysis, the coarse samples were ground into a powder and then characterized by XRD. X-ray results of the unmilled sample at 880 °C (Fig. 4- a) indicates the sharp peaks of Al_2O_3 phase and low intensity peaks of unreacted powders (remaining Al, $H_3BO_3$and C). Based on the XRD pattern

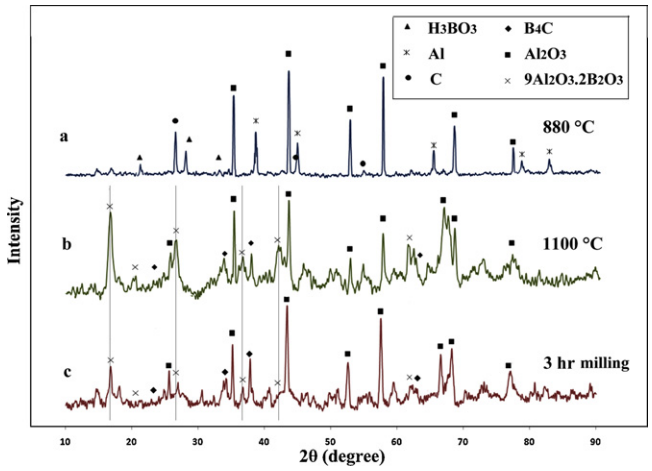

Fig. 4. XRD patterns for the DTA samples of (a) unmilled sample and heated up to 880 °C, (b) unmilled sample and heated up to 1100 °C, (c) sample milled for 3 h and heated up to 1100 °C.

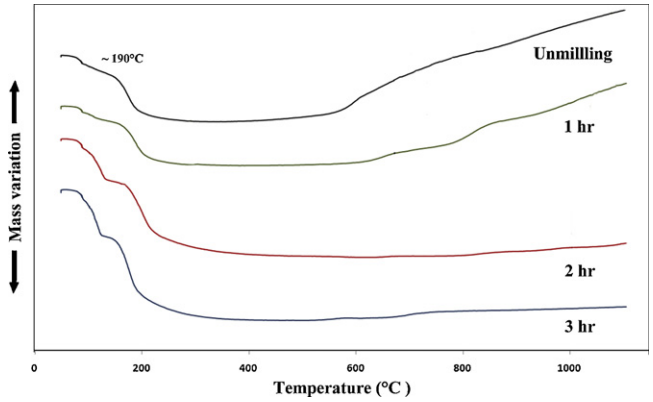

Fig. 5. TG curves for the $Al + H_3BO_3 + C$ mixtures milled at different times (heating rate 10 deg min^{-1}).

and thermodynamic analysis, the exothermic reaction taking place about 830 °C were related to the beginning of reduction of boron oxide by Al according to reaction (3). The XRD pattern of unmilled sample at 1100 °C presented in Fig. 4(b) exhibits that the remaining peaks corresponding to H_3BO_3 and C have completely been diminished, and several new peaks appear to emerge beside sharp peaks of Al_2O_3, corresponding to the formation of B_4C and aluminum borate (JCPDS: 00-009-0248). $9Al_2O_3{\cdot}2B_2O_3$ appears as the major by-product in the Al–B_2O_3–C system [14]. As a result, two exothermic peaks in the temperature range of 900–1100 °C resulted from the two reactions: (i) boron resulted from aluminothermic reaction and C reacted according to reaction (5) and B_4C formed, (ii) direct reaction happens between Al_2O_3 and remained B_2O_3 according to reaction (8).

$$9Al_2O_3 + 2B_2O_3 = 9Al_2O_3.2B_2O_3 \quad (8)$$

The DTA curve of 1 h milled sample shows similar thermal behavior of unmilled sample. As can be seen, the first exothermic reaction started around 640 °C before melting point of Al. It can be concluded that 1 h mechanical activation leads to shift aluminothermic peak and other exothermic reaction, respectively toward low temperatures. By increasing milling time to 2 h, DTA curve indicates two exothermic peaks which are partly overlapped and are located at about 640 °C and 680 °C, respectively. That is to say, when the first reaction takes place (aluminothermic reaction), its reaction heat will activate the next reactions (synthesis reaction) to occur subsequently. After mechanical activation for 3 h, there is only a wide and highly strong exothermic peak in the DTA curve as shown in Fig. 3. This shows that all the reactions happen almost at the same time. Also, it can be seen that the temperature of exothermic reaction shifts toward 590 °C. The reason for these may be that the mechanical activation can reduce the reaction distance due to microstructural refinement and accelerate the diffusion process. As a result, in this case, the ignition temperature of aluminothermic reaction decreases significantly. Moreover, mechanochemical processing can make reactions simultaneous via: (i) large amount of reaction heat, (ii) high active boron atoms produced by the aluminothermic reaction, and (iii) uniform distribution of C powder due to 3 h milling process.

The XRD pattern of 3 h milling sample at 1100 °C indicates sharp peaks of Al_2O_3 and B_4C peaks. In addition, after 3 h of milling, the intensity of peaks at around $2\theta = 16.619°$, $2\theta = 26.587°$, $2\theta = 35.966°$ and $2\theta = 41.544°$ decreased extremely indicating that the formation of aluminum borate would be decreased with an increase in milling time. The quantity of aluminum borate mainly depends on excess B_2O_3 in the system and is affected by the size of the B_2O_3 powder [14]. The excellent dispersion of powder in mechanochemical process at higher milling times helps consume B_2O_3, and

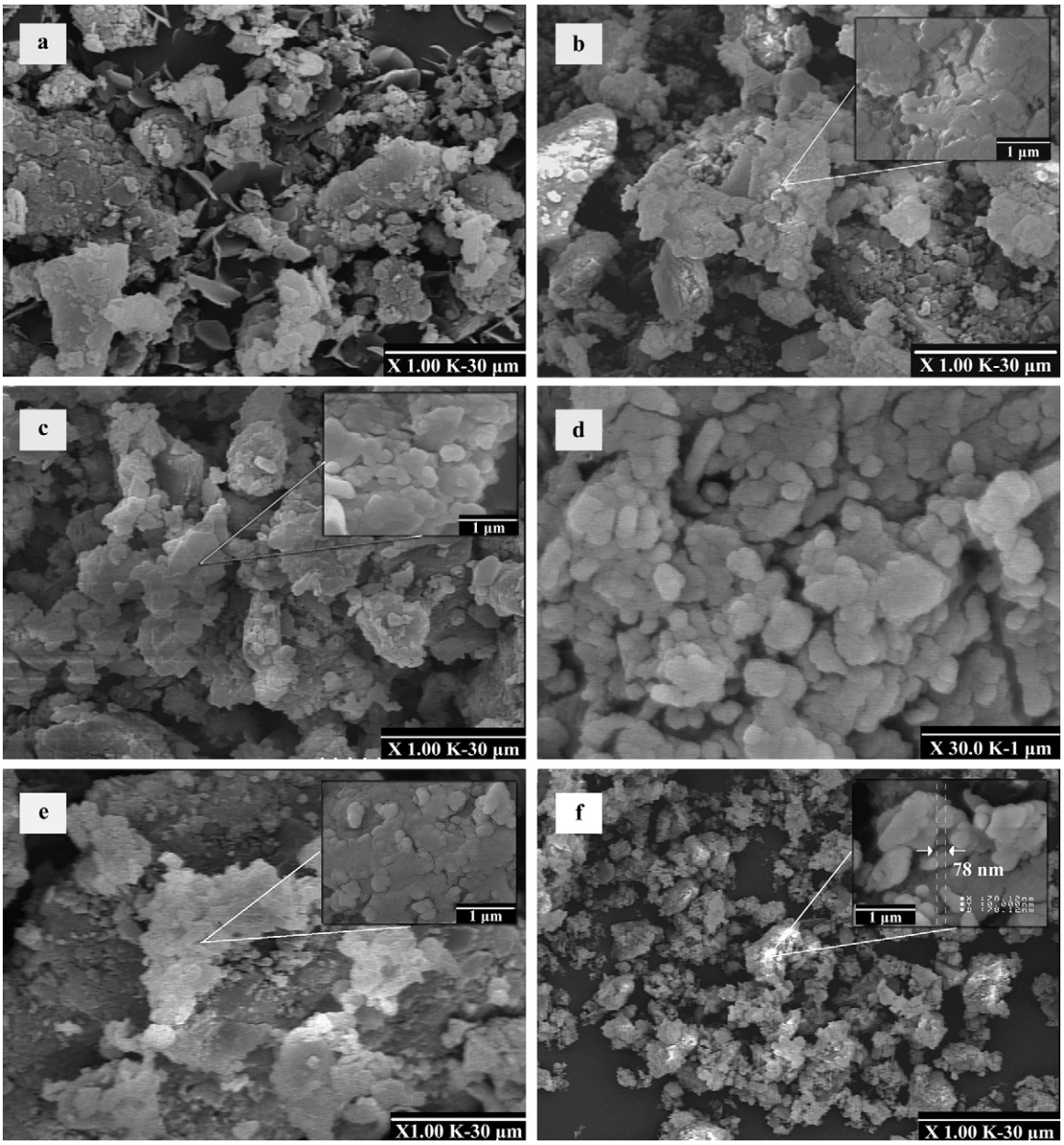

Fig. 6. SEM micrographs for the (a) raw materials (before milling), and the samples milled for (b) 1 h, (c) 2 h (d) 3 h, (e) 4 h and (f) 10 h.

decrease the particle size of B_2O_3 powder to prevent the formation of $9Al_2O_3{\cdot}2B_2O_3$. In addition, increasing the milling time could provide enough energy to decompose aluminum borate to Al_2O_3 and B_2O_3. This result, coupled with occurrence of all reactions at room temperature indicates that mechanosynthesis process is an effective route to synthesize Al_2O_3/B_4C composite with high purity.

Based on DTA analysis, 3 h milling process of starting mixtures leads to a change in the reaction mechanism from a three-step exothermic reaction to one-step low-temperature reaction. This fact, quick transformation observed by XRD analysis (Fig. 1) and high T_{ad} calculated by thermodynamic relations (Table 3) can reveal the synthesis of Al_2O_3/B_4C composite via mechanochemical method which occurred in MSR mode.

TG curves of the powders with different milling times are shown in Fig. 5. The decrease region in TG curve near 190 °C can be related to dissociation of boric acid to boron oxide and water vapor. The increase region in TG diagram of unmilled and 1 h milled samples can be proposed to formation of large amount of $9Al_2O_3{\cdot}2B_2O_3$. Some researchers reported that by increasing the milling time, the exothermic aluminothermic reaction provided the required heat for the carbothermic reactions [25,26]. As can be seen, the TG curve does not show any significant change in the sample weight after 200 °C, and this indicated that there is no gas (CO or CO_2) emission during the combustion synthesis. Also, carbothermal reaction (4) is sensitively endothermic thermodynamically, but there is no endothermic peak corresponding to carbothermal reaction in DTA curves. In addition, carbothermal reaction could be achieved at high-temperature; due to diffusional mechanism and low rate of heat conduction, which needs a long time [25]. Based on these results, we can conclude that the carbothermal reaction did not occur during milling process of $Al–B_2O_3–C$ system.

3.4. Morphology

In this case, before 4 h of milling time, the system involved three ductile and soft powders (Al, H_3BO_3 and C); but after 4 h, ductile

system changed to brittle–brittle system by forming the ceramic components (Al_2O_3 and B_4C). Fig. 6 shows SEM micrographs for the raw materials (before milling), and the samples milled for 1, 2, 3, 4 and 10 h. As can be seen clearly in Fig. 6(a), the as-received aluminum powder particles were irregular in shape with a size distribution of 20–100 μm. The graphite particles had flak shapes with a size distribution of 30–50 μm. After 1 h milling process, the aluminum powder particles get flattened to platelet/pancake shapes by a micro-forging process (Fig. 6b). By increasing milling time to 2 h, in the next step, cold welding of the flattened particles gets started and makes lamellar shaped structures (Fig. 6c). It can be confirmed by intensities of the main peaks of the aluminum that did not change with increasing the milling time to 3 h (Fig. 1). After 3 h milling process, the steady state stage is achieved when the average particle size distribution is narrow and gets homogenized in size and shape as reported by some researchers (Fig. 6d)[8,27]. This phenomenon happened when the rate of the cold welding mechanism leading to larger particle size, and the rate of the fraction mechanism leading to smaller particle size, were equal [8]. In this stage, due to heavy deformation introduced into the particles, variety of crystal defects such as dislocations, vacancies, stacking faults and number of grain boundaries extensively increased. The presence of these defects, coupled with the refined microstructure can decrease the diffusion distances providing required mechanical activation for the combustion reaction to be initiated. Combustion type reactions in most cases produce coarse product particles owing to the rapid evolution of reaction heat [6]. Additionally, with further milling, reduction of the particle size and increase in the number of defects areas lead to make of new additional unstable surface. Thus, the agglomeration phenomenon occurred to diminish surfaces and to decrease the surface energy [16]. The morphology of powder particles after combustion reaction, i.e. 4 h of milling time, is shown in Fig. 6(e). As can be seen, due to the heat released by the combustion reaction and the unstable surface enhanced by reduction of particle size, the powder particles adhere together and make large agglomerations. By increasing milling time to 10 h, the system changed into brittle–brittle (Al_2O_3–B_4C) component (Fig. 6f). Brittle components get fragmented during milling and their particle size gets reduced continuously. Therefore, significant decrease in agglomerate and particle sizes occurred as can be observed in Fig. 6(f). The range of powder size which agglomerated is below 100 nm.

4. Conclusion

To sum up, ceramic matrix nanocomposite Al_2O_3/B_4C has been synthesized by using commercial pure materials Al, H_3BO_3 and C (graphite) and mechanical activation of precursor materials. The results of this research work can be summarized as follows:

High T_{ad} calculated by thermodynamic relations, quick transformation observed by XRD analysis and one-step exothermic reaction seen in DTA analysis can reveal the synthesis of Al_2O_3/B_4C composite via mechanochemical method which occurred in MSR mode.

The phase detection exhibits that no traces of the product phases in the 3 h milling, while increasing milling time to 4 h led to the occurrence of reactions with combustion mode; as a result, Al_2O_3/B_4C nanocomposite powder was formed. Further milling process up to 10 h had no special effect except broadening of Bragg peaks which is ascribed by decreasing the crystallite size.

Based on TG–DTA analysis, the aluminothermic reaction takes place after melting point of aluminum in unmilled sample which leads to the formation of B_4C and $9Al_2O_3{\cdot}2B_2O_3$. By increasing the milling time to 3 h, an exothermic reaction takes place before aluminum melting in a solid state condition. Moreover, the quantity of $9Al_2O_3{\cdot}2B_2O_3$ extremely decreases with an increase in milling time.

The SEM micrographs show that after 4 h milling, the powder particles adhere together and make large agglomerations. By increasing the milling time to 10 h, the average particle size distribution is narrow, and gets homogenized in size. The average particle size is below 100 nm.

Acknowledgements

The authors would like to thank the research affairs of Islamic Azad University, Najafabad branch for financial support of this research.

References

[1] X.L. Shi, F.M. Xu, Z.J. Zhang, Y.L. Dong, Y. Tan, L. Wang, J.M. Yang, Mater. Sci. Eng. A. 527 (2010) 4646–4649.
[2] S.P. Liu, K. Ando, B.S. Kim, K. Takahashi, Int. Commun. Heat Mass Transfer 36 (2009) 563–568.
[3] V.R. Khrustov, V.V. Ivanov, Yu.A. Kotov, A.S. Kaigorodov, O.F. Ivanova, Glass Phys. Chem. 33 (2007) 379–386.
[4] M.A. Khaghani-Dehaghani, R. Ebrahimi-Kahrizsangi, N. Setoudeh, B. Nasiri-Tabrizi, Int. J. Refract. Met. Hard Mater. 29 (2011) 244–249.
[5] M. Sternitzke, J. Eur. Ceram. Soc. 17 (1997) 1061–1082.
[6] B.S.B. Reddy, K. Das, S. Das, J. Mater. Sci. 42 (2007) 9366–9378.
[7] S.C. Tjong, Z.Y. Ma, Mater. Sci. Eng. 29 (2000) 49–113.
[8] C. Suryanarayana, Mater. Sci. 46 (2001) 1–184.
[9] A.K. Suri, J.K. Subramanian, T.S.R.C. Murthy, Int. Mater. Rev. 55 (2010) 4–40.
[10] X. Lin, P. Darrell Ownby, J. Mater. Sci. 35 (2000) 411–418.
[11] C.H. Jung, S.J. Lee, Int. J. Refract. Met. Hard Mater. 23 (2005) 171–173.
[12] H.C. Yi, J.Y. Guigné, L.A. Robinson, A.R. Manerbino, J.J. Moore, J. Porous Mater. 11 (2004) 5–14.
[13] L. Yonghe, Y. Sheng, Z. Weijing, L. Hoyi, Scripta Mater. 39 (1998) 1237–1242.
[14] Y. Liu, S. Yin, Z. Guo, L. Hoyi, J. Mater. Res. 13 (1998) 1749–1752.
[15] D. Chaira, B.K. Mishra, S. Sangal, Sci. Eng. A. 460–461 (460) (2007) 111–120.
[16] P. Balaz, Mechanochemistry in nanoscience and minerals engineering, first ed, Springer, Berlin Heidelberg, Germany, 2008.
[17] S. Mondal, A.K. Banthia, J. Eur. Ceram. Soc. 25 (2005) 287–291.
[18] I. Yanase, R. Ogawara, H. Kobayashi, Mater. Lett. 63 (2009) 91–93.
[19] H. Werheit, A. Leithe-Jasper, T. Tanaka, H.W. Rotter, K.A. Schwetz, J. Solid State Chem. 177 (2004) 575–579.
[20] E. Pascual, E. Martínez, J. Esteve, A. Lousa, Diam. Relat. Mater. 8 (1999) 402–405.
[21] V. Sabari Giri, R. Sarathi, S.R. Chakravarthy, C. Venkataseshaiah, Mater. Lett. 58 (2004) 1047–1050.
[22] S. Das, S. Datta, A.K. Mukhopadhyay, K.S. Pal, D. Basu, Mater. Chem. Phys. 122 (2010) 574–581.
[23] L. Takacs, Int. J. SHS 18 (2009) 276–282.
[24] O. Kubaschewski, C.B. Alcock, Metallurgical thermochemistry, fifth ed., Pergamon Press, UK, 1979.
[25] M. Sakaki, M.Sh. Bafghi, J. Vahdati Khaki, Q. Zhang, F. Saito, J. Alloy Compd. 486 (2009) 486–491.
[26] M.S. Marashi, J. Vahdati Khaki, J. Alloy Compd. 482 (2009) 522–525.
[27] C.L.D. Castro, B.S. Mitchell, in: M.I. Baraton (Ed.), Synthesis functionalization and surface treatment of nanoparticles, American Scientific, USA, 2002, pp. 1–15.